ARTICLES

Analytical Free Energy Minimization of Silica Polymorphs

Julian D. Gale

Department of Chemistry, Imperial College of Science, Technology and Medicine, South Kensington, SW7 2AY, U.K.

Received: December 3, 1997; In Final Form: February 27, 1998

Free energy minimization based upon analytical, rather than numerical, derivatives has been applied for the first time to quartz and microporous silica polymorphs. To maximize the efficiency of this method to make the study of large unit cells practical, while maintaining accuracy, a new set of shell model parameters have been derived based on the properties of α-quartz which avoid the need for genuine three-body terms. Full minimization of the free energy with respect to both strains and internal degrees of freedom is found to lead to soft modes at about room temperature in the absence of anharmonic corrections, and therefore analytical free energy minimization within the zero static internal stress approximation is found to be the preferred method for quartz and microporous materials. The wider implication is that total free energy minimization in the quasiharmonic approximation of complex chemical systems is likely to fail at relatively modest temperatures and before the classical limit is reached.

1. Introduction

Silicates and their derivatives are very important materials in many areas of science. At the high-density end of the range of silica polymorphs we have quartz, coesite, and stishovite, which are important in mineralogy,[1] while at the lower density end there are an everincreasing number of microporous and mesoporous, silicates.[2] Such porous forms play a pivotal role in many forms of shape selective catalysis as well as other applications such as ion exchange and molecular sieving.[3]

For many years there has been a strong interest in being able to model the structure and properties of silicate minerals using computational techniques as a complement to experiment. Despite the increasing scope of quantum mechanical methods, interatomic potentials still represent a valuable tool for modeling silicate structures. In fact some potentials, such as the shell model potential of Sanders et al.,[4] have proved to be as reliable for unit cell parameters as many quantum mechanical methods.

One of the key aims of computer modeling of silicates is to be able to predict structures and properties as a function of both pressure and temperature. In a mineralogical context this is particularly crucial as many minerals exist under extreme conditions that are difficult to simulate in the laboratory, while in a chemical context it is useful to know how the structure of a heterogeneous catalyst changes under reaction conditions.

Inclusion of pressure into an energy minimization is trivial, as this only requires the addition of the term *PV* to the internal energy, which is normally calculated, to make the objective quantity the enthalpy. Introducing temperature into a simulation is more complex, and there are several approaches that can be utilized. Two standard techniques for modeling systems at finite temperature are molecular dynamics[5] and Monte Carlo methods.[6] Both represent numerical integration of the system properties to determine the ensemble average, the former having the additional advantage that information in the time domain is also yielded, though typically only for small amounts of real time. While both methods are very useful for many problems, they have two disadvantages. First, they are only strictly valid for solids at elevated temperatures as they neglect the effect of vibrational quantum effects, such as the zero-point energy. For many minerals the heat capacity only truly obeys the classical Dulong−Petit result at in excess of 1000 K,[7] which is sometimes higher than the conditions often used for experimental studies. Second, the statistical uncertainty in the ensemble averages only decreases as the inverse square root of the simulation size, be this run length or number of atoms. Hence, numerical integration also represents a relatively expensive route to simulating the effect of temperature when the ions in a system are principally just vibrating about their lattice sites.

The free energy of a solid can readily be calculated using statistical mechanics through the vibrational partition function. Hence this offers an attractive route to simulating the properties of materials as a function of temperature by minimizing the free energy instead of the internal energy. This approach removes the statistical uncertainty associated with the numerical integration and should be considerably faster. The main restriction is that it relies on the validity of the quasiharmonic approximation, which typically restricts the temperature range that can be studied to about half the melting point unless further corrections are included for anharmonicity.[8] Nonetheless, for ionic materials with high melting points this covers many of the conditions of interest except for phase transitions.

Historically the difficulty with minimizing the free energy has been to obtain the derivatives of the free energy with respect to the structural parameters. Hence the majority of the free energy minimization studies to date have relied on some degree of approximation. A number of schemes have been proposed recently for practical calculations. Sutton[9] has developed the

S1089-5647(98)00396-4 CCC: $15.00
Published on Web 06/23/1998

idea of Montroll[10] by using the moments of the dynamical matrix with an approximate functional form for the phonon density of states which has the correct asymptotic limits to produce an analytic expression for the free energy. This avoids the need for matrix diagonalization and allows straightforward differentiation to be performed. Srolovitz and co-workers have introduced a variational approach which integrates the potential function over a Gaussian distribution that depends on the temperature.[11] Both of these methods have been used primarily for the study of metals and alloys so far.

Within the silicate field, Parker and co-workers have used free energy minimization with success for modeling thermal expansion.[12,13] Their approach is based on the assumption that the dominant effect of temperature is on the unit cell dimensions, rather than the internal fractional coordinates. If this is the case, then it becomes feasible to numerically determine the strain derivatives of the free energy by finite differences, as there are at most six components to evaluate, and for many materials, with symmetry taken into account, there may be considerably less than this.

Recently a method has been proposed that directly determines the free energy forces analytically from the derivatives of the dynamical matrix.[14] In this work we aim to explore whether it is possible to use this approach efficiently for the study of silicate structures as a function of temperature and whether the full minimization of the free energy, including with respect to the internal degrees of freedom, has a significant influence on the results obtained. If successful, this method has important implications for the study of complex systems, such as molecular crystals, in the low-temperature regime which have not traditionally been studied by free energy minimization. Furthermore, problems such as low-temperature adsorption within microporous materials and at surfaces could be studied once the effect of the free energy on equilibrium position is no longer restricted to unit cell dimensions by practical considerations.

2. Methods

The theory behind the analytical free energy minimization method was recently developed by Kantorovich and applied to alkali halide crystals.[14,15] Subsequently the method has been refined by Taylor et al., who have discussed many of the details of its implemenation.[16] However, as the approach is relatively new, a summary of the main features will be given here. When referring to the free energy in this work we will be primarily concerned with the Helmholtz free energy. However, in the absence of an externally applied pressure this will be equivalent to the Gibbs free energy when calculated at the minimum Helmholtz free energy configuration. In the presence of an externally applied pressure then the free energy calculated will be the Gibbs free energy, but again only after free energy minimization.

The Helmholtz free energy can be written as the sum of the static internal energy, U_{static}, that would be calculated in a conventional energy minimization, the vibrational energy, U_{vib}, and the term arising from the vibrational entropy, S_{vib}:

$$\mathrm{A} = U_{\text{static}} + U_{\text{vib}} - TS_{\text{vib}}$$

This assumes that there is no contribution from configurational disorder that must be corrected for separately. For convenience we can express the sum of the vibrational energy and entropy term together, due to the cancellation of a common term, as

$$U_{\text{vib}} - TS_{\text{vib}} = \sum_k \sum_m \left\{ \frac{1}{2} h\omega_m(k) + kT \ln\left[1 - \exp\left(- \frac{h\omega_m(k)}{kT} \right) \right] \right\}$$

where the sum over K points is used to approximate the integral over the Brillouin zone of the phonon density of states. This point will be discussed further, later. The vibrational frequencies at each K point are given by the square root of the eigenvalues of the dynamical matrix, which in turn are related to the phased second-derivative matrix multiplied by vectors containing the inverse square root of the atomic masses:

$$\omega^2(k) = e^{-1}(k)\, D(k)\, e(k)$$

$$D^{ij}_{\alpha\beta}(k) = \frac{1}{(m_i m_j)^{1/2}} \sum_1 \left(\frac{\partial^2 U_{\text{static}}}{\partial\alpha\, \partial\beta} \right) \exp(\mathrm{i}k(r_{ji} - r_{i0}))$$

The derivatives of the free energy with respect to structural parameters can be related to the derivatives of the eigenvalues or frequencies squared:

$$\left(\frac{\partial A}{\partial \epsilon} \right) = \left(\frac{\partial U_{\text{static}}}{\partial \epsilon} \right) + \sum_k \sum_m \left\{ \frac{h}{2\omega_m(k)} \left(\frac{1}{2} + \frac{1}{\exp(h\omega_m(k)/kT) - 1} \right) \left(\frac{\partial \omega^2}{\partial \epsilon} \right) \right\}$$

Hence the key is to obtain the derivatives of the eigenvalues. Through the application of perturbation theory these derivatives can be related to derivatives of the elements of the dynamical matrix projected onto the eigenvectors of each phonon mode:

$$\left(\frac{\partial \omega^2}{\partial \epsilon} \right) = e^*_m(k) \left(\frac{\partial D(k)}{\partial \epsilon} \right) e_m(k)$$

The first derivatives of the dynamical matrix elements are just the third derivatives with respect to either three Cartesian coordinates, for internal degrees of freedom, or two Cartesian coordinates and the external strain in the case of the unit cell derivatives. Both must also be multiplied by the appropriate phase factor for the point in the Brillouin zone.

Although the determination of the first derivatives of the free energy in this way is in principle straightforward, the difficulty lies in making an efficient implementation so that calculations are practical for moderately large systems. The first dilemma is that the second-derivative terms are needed both to calculate the dynamical matrix and to generate the third derivatives. However, the third derivatives cannot be utilized until the eigenvectors are known, which is after the dynamical matrix has been completely built and diagonalized. Furthermore there is duplication in the work between the calculation of the static contributions and the building of the dynamical matrix. It is impractical to store all the completed third derivatives for use later, as the amount of memory required would be beyond the current generation of computers. Taylor et al. have implemented a scheme where a number of intermediate terms are stored between various stages of the calculation as a compromise between computational efficiency and memory usage.[16]

In the implementation used in this work no terms are stored so that the calculations can be performed in the minimum amount of memory, which is the same as for a phonon calculation alone in the limit of large systems. The second-derivative storage, which dominates the memory for large

systems, requires $4 \times (3N)^2$ double precision floating point numbers for the calculation of the phonons at a general K point or half this amount at the gamma point, where no complex arithmetic is required. Allowing also for the lower half triangular Hessian, the total amount of memory needed in this algorithm is approximately $324 \times N^2$ bytes, which compares to $2000 \times N^2$ bytes in the algorithm of Taylor et al.[17] As the calculation of the dynamical matrix is at worst an N^2 process and the static components can be efficiently calculated using symmetry-adapted algorithms, the penalty for duplicating the calculation of terms is not severe. This phase of the calculation dominates the CPU time only for small systems, where the calculations are quick anyway.

An approach that could lead to some improved efficiency during geometry optimization is to calculate the free energy derivatives based on the eigenvectors from the previous step. Initially this would lead to an error in the derivatives, but as the calculation converges to the minimum energy configuration, the effects of the approximation would decrease as the scheme reaches self-consistency.

One important observation is that to get good performance in the calculation of the derivatives, it is essential to optimize the division of work between real and reciprocal space. Jackson and Catlow have given a derivation of the formula for the optimum partitioning.[18] However, this assumes that the calculation of a term in real and reciprocal space costs the same amount. In practice as the order of the derivatives increases, it becomes more efficient to calculate terms in real space, whereas for the energy alone reciprocal space is more efficient as it can be formulated as an order N process.

For large systems there are two parts of the calculation which scale as N^3 and therefore potentially dominate the computational expense. The first is the diagonalization of the complex Hermitian dynamical matrix, for which there are already efficient libraries of routines. The second is the projection of the third derivatives by multiplication with the eigenvectors for each phonon mode. This second part can potentially be a bottleneck for large systems, and therefore it is crucial to minimize the number of multiplication operations. By doing this carefully, the prefactor for this part can be reduced by more than an order of magnitude. As a result, the matrix diagonalization always becomes the dominant expense with increasing numbers of atoms, unless Hessian recalculation is required frequently, in which case matrix inversion becomes the limiting factor.

Typically the evaluation of a single-point free energy and gradients requires twice the amount of CPU time as a phonon calculation including eigenvectors for small systems. This ratio decreases with increasing N so that by the time a few hundred atoms are being considered the extra cost is only about 40%, with potential for further savings from the use of symmetry. If we contrast this with numerical evaluation of the free energy derivatives using central finite differences, this requires $2N_v + 1$ phonon calculations with a constant volume optimization at each point, where N_v is the number of strain variables. Clearly analytical evaluation of the derivatives will therefore be faster, given the above timings, even for the case of a single strain variable. Furthermore, analytically the cost has negligible dependence on the number of variables whose derivatives are required.

Having obtained the first derivatives of the free energy, we need to be able to efficiently optimize the geometry of the system with respect to this quantity. Here we follow the approach of Taylor et al., which is to use a Newton−Raphson method based on an approximate Hessian matrix which is calculated from the static second derivatives only.[16] This matrix is updated subsequently using the BFGS scheme, which will, in principle, tend to correct for the missing vibration contribution over sufficient cycles. In practice, the static Hessian is already a good approximation, and so only a few a cycles of minimization are required when starting from the statically optimized structure.

The above scheme generates both internal and external derivatives with respect to the free energy. However, for comparison we would also like to be able to perform calculations within the zero static internal stress approximation (ZSISA), in the notation of Taylor et al., as used previously in the numerical formulation. In this case the internal variables must be minimized with respect to the internal energy while only the strain variables are minimized with respect to the free energy. To achieve this, we must first neglect the thermal contribution to the internal forces. However, there will also be a correction term arising for the strain derivatives associated with the fact that the internal energy must remain at its minimum point as the cell is strained.[19] This is analogous to the internal second-derivative contribution to the elastic constant tensor.

The strain correction can be derived simply as follows. The free energy can be expanded about the current structure with respect to strain as a Taylor series:

$$A(\mathrm{d}\epsilon) = A(0) + \frac{\mathrm{d}A}{\mathrm{d}\epsilon}\mathrm{d}\epsilon + \frac{\mathrm{d}^2A}{\mathrm{d}\epsilon\,\mathrm{d}\alpha}\mathrm{d}\alpha\,\mathrm{d}\epsilon + \frac{\mathrm{d}^2A}{\mathrm{d}\epsilon^2}(\mathrm{d}\epsilon)^2 + \ldots$$

If we collect together terms in $\mathrm{d}\epsilon$, then the ZSISA strain derivative can be seen to be

$$\left(\frac{\mathrm{d}A}{\mathrm{d}\epsilon}\right)_{\mathrm{ZSISA}} = \frac{\mathrm{d}A}{\mathrm{d}\epsilon} + \frac{\mathrm{d}^2A}{\mathrm{d}\epsilon\,\mathrm{d}\alpha}\mathrm{d}\alpha$$

Using the standard result for the estimate of the internal displacements required to reach the minimum energy coordinates that comes from Newton−Raphson minimization, we now obtain the following result:

$$\left(\frac{\mathrm{d}A}{\mathrm{d}\epsilon}\right)_{\mathrm{ZSISA}} = \frac{\mathrm{d}A}{\mathrm{d}\epsilon} - \frac{\mathrm{d}^2A}{\mathrm{d}\epsilon\,\mathrm{d}\alpha}\left(\frac{\mathrm{d}^2A}{\mathrm{d}\alpha\,\mathrm{d}\beta}\right)^{-1}\frac{\mathrm{d}A}{\mathrm{d}\beta}$$

As we wish to avoid calculating the second derivatives with respect to the free energy due to the complexity and computational cost, we can approximate the two second-derivative matrices by the static-only components. Because one matrix is multiplied by the inverse of the other, there will be a significant cancellation of errors, and this turns out to be a good approximation in practice.

All calculations in this study have been performed using the program GULP.[20] The symmetry features of the program are used to restrict geometry optimizations to the asymmetric unit variables, although at this stage no attempt is made to use symmetry to accelerate the calculation of the free energy derivatives. Previous results suggest that quite a substantial benefit should be gained from implementing this in the future.

Integrations across the Brillouin zone for the calculation of phonons use the Monkhorst−Pack scheme, in which a grid is specified by the number of points along each axis, with the mesh being offset from the gamma point.[21] As the minimum memory algorithm has been implemented, the computational cost scales approximately linearly with the number of K points sampled when the number is large. To improve this aspect, the mesh points are restricted to the asymmetric wedge of the Brillouin

zone, with appropriate weighting, as this can significantly reduce the number of K points required.[22]

3. Results and Discussion

3.1. Derivation of Interatomic Potentials. There have been a large number of interatomic potential sets derived for the modeling of silicates, both by empirical means and increasingly from ab initio calculations in recent years.[23,24] One of the most successful potentials has been that of Sanders et al.,[4] who fitted the properties of α-quartz using formal ionic charges, a shell model[25] to represent the polarizability of oxygen, and a Buckingham potential to model short-range repulsion and dispersive attraction. In addition, a three-body potential was found to be beneficial for the O−Si−O angle, which is relatively rigid in most silicates when compared to Si−O−Si, which is rather flexible.

In recent years there have been several reparametrizations based on the above model which have used ab initio cluster calculations to determine the constants.[26] While this is important for embedded cluster calculations,[27] so that the force field and quantum mechanical method are as consistent as possible, there is no clear improvement over the empirical parametrization for most aspects of silicate modeling. One thing that is clear, though, is that it is important to account for the polarizability of oxygen, as this leads to the stabilization of low-symmetry distortions, such as the monoclinic structure of silicalite at low temperatures.[28]

When we come to select the best interatomic potential set for use in the free energy minimization of silicates, there are a number of criteria to consider. In addition to the usual factors taken into consideration for an athermal calculation, such as the accuracy of the reproduction of structures and phonon frequencies, we must also now consider the computational efficiency given the significant increase in computational cost. It turns out that the use of a general three-body term is particularly disadvantageous for free energy minimization as the number of eigenvector projections of the third derivatives increases significantly and this step can potentially scale as N^4 if all atoms were to interact via three-body terms. Hence it is desirable to use a potential model that retains the benefits of the shell model, but without the disadvantages of three-body terms. It turns out that this goal can be achieved by using a Urey−Bradley three-body term instead of the standard harmonic angle form:

$$\text{Urey−Bradley:} \qquad E = (1/2)K_{ub}(r_{213} - r_0)^2$$

$$\text{Harmonic angle:} \qquad E = (1/2)K_2(\theta - \theta_0)^2$$

Because the angle between two bonds is a function of all three bond lengths, it cannot be reduced to a two-body interaction. However, the Urey−Bradley form is already a two-body potential, except that it is only applied when the two terminal atoms, in this case oxygen, have a common bonded atom of the required type, i.e., silicon.

To obtain a silicate force field that matches the accuracy of the empirical shell model potential but while maximizing the computational efficiency, we have reparametrized this model using the Urey−Bradley three-body potential. Following the original procedure, the parameters have been derived by relaxed fitting[29] to both the structure of α-quartz and selected properties, which include the on-diagonal elastic constants and the static and high-frequency dielectric constants. The optimized parameter set is given in Table 1.

TABLE 1: Fitted Shell Model Potential Parameters Based on α-Quartz[a]

interaction	A (eV)	ρ (Å)	C (eV Å^6)	K_{cs} (eV Å^{-2})	K_{ub} (eV Å^{-2})	r_0 (Å)
Si−O$_s$	1277.514	0.32052	5.9062			
O$_s$−O$_s$	22764.0	0.14900	27.879			
O$_c$−O$_s$				79.074		
O$_s$−Si−O$_s$					2.30273	2.43352

[a] Here the parameters A, ρ, and C are the coefficients of a Buckingham potential ($E = A\exp(-r/\rho) - Cr^{-6}$), K_{cs} is a core-shell spring constant, and K_{ub} and r_0 are the parameters of the Urey−Bradley potential, as given in the main text. The charges are +4.0 for Si, which is a rigid ion, +0.86902 for O Core (O$_c$), and −2.86902 for O Shell (O$_s$). The cutoff used for the Buckingham potentials was 12.0 Å, while the maximum Os−Os distance allowed for the Urey−Bradley potential was 2.8 Å.

TABLE 2: Comparison of the Experimental Structure[30] and Properties[31,32] of α-Quartz with Those Values Calculated by the Current Model and Also Those Obtained from the Sanders et al. Potential[4]

property	experimental	sanders model	this work
a (Å)	4.9021	4.8681	4.8989
c (Å)	5.3987	5.3738	5.4017
Si x (frac)	0.4680	0.4669	0.4660
O x (frac)	0.4124	0.4109	0.4133
O y (frac)	0.2712	0.2730	0.2713
O z (frac)	0.2170	0.2196	0.2163
C_{11} (GPa)	86.8	95.3	97.0
C_{13} (GPa)	11.9	18.1	18.6
C_{33} (GPa)	106.0	112.7	105.2
C_{44} (GPa)	58.3	49.8	48.0
C_{66} (GPa)	39.9	40.1	40.5
ϵ_{11}^0	4.52	4.58	4.81
ϵ_{33}^0	4.64	4.88	5.29
ϵ_{11}^∞	2.4	2.07	1.98
ϵ_{33}^∞	2.4	2.09	1.99
ν_{max} at Γ (cm^{-1})	1162	1021.2	1096.5

The new parameter set is found to be more accurate in reproducing the structure of quartz than the original values, as can be seen from the comparison of data given in Table 2. It should be noted that the structure chosen for fitting in this study is one measured at 13 K,[30] as the lowest temperature structure possible is most appropriate for the derivation of parameters for free energy minimization. The original Sanders potential was actually fitted to a room-temperature crystal structure. However, as quartz has a positive thermal expansion coefficient and the Sanders potential underestimates the cell parameters, this only makes the comparison more favorable for the new potential model.

In terms of the properties there is little to choose between the two parametrizations of the shell model, as both models are of similar quality in reproducing the elastic constants. Of particular importance in lattice dynamical calculations though are the phonon frequencies. The standard shell model potentials for both silicates and aluminophosphates have always fared worse than some rigid ion models in underestimating the high-frequency stretching modes at the gamma point, while doing better for the acoustic modes. One improvement in the present reparametrization is that the error in the high-frequency stretch has been halved.

The parameter set given in Table 1 represents the optimal set for athermal modeling, at least within the constraints of the allowed parameters and weighting factors used for the observables. However, the moment we switch to free energy minimization, even at 13 K, this will introduce errors in the calculated structural parameters due to the zero-point energy. Therefore it is necessary to slightly modify the parameters to

TABLE 3: Optimized Free Energy and Unit Cell Parameters for α-Quartz at 13 K as a Function of the Grid Size Used To Sample the Brillouin Zone. The Total Number of Symmetry Unique K Points Is Also Included for Comparison

grid size	number of K points	*a* (Å)	*c* (Å)	free energy (eV)
1 × 1 × 1	1	4.900 67	5.402 61	−381.879 07
2 × 2 × 2	3	4.900 22	5.402 13	−381.877 93
3 × 3 × 3	10	4.900 22	5.402 14	−381.878 05
4 × 4 × 4	20	4.900 22	5.402 15	−381.878 08
5 × 5 × 5	39	4.900 23	5.402 15	−381.878 10
6 × 6 × 6	63	4.900 23	5.402 15	−381.878 10

correct for this. The effect of the zero-point energy is to lead to a small expansion of the cell parameters. To compensate, we have decreased the dominant short-range repulsion term, A(Si−O), to a value of 1271.514 eV for use in free energy minimization while keeping all other the parameters fixed. This results in cell parameters of 4.9002 and 5.4022 Å for *a* and *c*, respectively, in α-quartz, which are similar to the athermal values.

3.2. Free Energy Minimization of α-Quartz. The thermal expansion and properties of α-quartz have been studied extensively, both experimentally and theoretically.[33,34] Here we will briefly consider this material again to examine both the performance of the new shell model reparametrization and in order to compare the results obtained from complete free energy minimization with those calculated within ZSISA.

First, we need to examine the convergence of the Brillouin zone integration scheme to establish the required grid size. In Table 3 the optimized unit cell parameters and free energy at 13 K are given for increasing grid sizes. Because of the similarity of the *a* and *c* cell parameters for quartz, the same number of mesh points were selected along each axis. A grid of 5 × 5 × 5 leading to 39 symmetry unique K points is found to be sufficient to converge all the observables to the required accuracy.

Free energy minimization was performed for α-quartz at 13 K, 50 K, and subsequently at intervals of 50 K up to 1000 K. Both full minimization of the free energy with respect to strains and fractional coordinates and minimization only within ZSISA were performed, and the results are plotted in Figure 1. For more detailed comparison, structural parameters are compared with experiment at 13 and 296 K in Table 4. In reality, α-quartz undergoes a transition to *β*-quartz in the region of 846 K, which is not directly reproduced by the lattice dynamics, as it involves disordering of the oxygen atoms over two different sites with partial occupancies of a half each.[35]

Direct comparison of the lattice parameters with experiment at the two temperatures in Table 4 must be made with care, as the order of magnitude of the change in the structural parameters over this temperature range is comparable to the errors in the cell parameters due to the limitations of the force field, even though the latter are quite small. The best measure is the change in the parameters due to heating, also shown in Table 4. From these we can see that ZSISA tends to lead to an underestimation of the changes by roughly a factor of 2, while full free energy minimization leads to an overestimation of the internal shifts by about 50%, but gives improved reproduction of the cell parameter changes. Given that the potential model overestimates the principal elastic constants, we would expect the thermal expansion of the cell to be underestimated. Hence, we cannot take the better agreement of full free energy minimization with experiment as necessarily indicative of superiority. Both the Sanders model and the Jackson and Catlow[18] variant of it give similar values for the cell parameter change along the *a* axis to the present model, in the zero static internal stress approximation, but are worse in the *c* direction.

In Figure 1, where the unit cell parameters are plotted over a range of temperatures, the most striking feature is that the curve for full free energy minimization terminates at room temperature. Beyond this point full free energy minimization fails due to the appearance of soft modes in the Brillouin zone which ultimately become imaginary. Because the internal degrees of freedom are being minimized with respect to the free energy, this drives the formation of soft modes, as small frequencies have the largest effect on lowering the free energy. For all the silicates we have tested this effect becomes catastrophic at about room temperature, leading to the breakdown of the method. In contrast, ZSISA never suffers from the same difficulty, as only the strains are minimized with respect to the free energy, which tends to lead to a uniform scaling of frequencies. This failure can be attributed to the method, as the same effect is observed with a range of different interatomic potentials from the literature, both rigid ion and shell model. In addition, it is important to note that the same potentials do not fail at room temperature when used in a molecular dynamics simulation

In previous studies where the internal degrees of freedom have been minimized with respect to the free energy no such problems have been observed.[36] However, the systems studied have usually been high-symmetry ionic materials with limited internal freedom and no facile distortions which can enhance the softening of modes. It appears that in materials where there are low-frequency modes due to the rotation of polyhedra or molecular fragments complete free energy minimization in the above formulation is not reliable except at very low temperatures. To extend the range of applicability, it is essential to include the effects of anharmonicity as by moving the ions away from the minimum with respect to the static energy higher order terms rapidly become crucial.

As a consequence of the above, only free energy minimization in the zero static internal stress approximation will be considered in the remainder of this work. One final point should be made: if free energy minimization is performed by just neglecting the lattice dynamical contribution to internal derivatives, this does not lead to true minimization ZSISA. In other words, the correction term for the strain derivatives given in section 2 makes a significant contribution. In the case of quartz, neglecting this term leads to a negative thermal expansion coefficient, which is incorrect for this material.

3.3. Free Energy Minimization of Microporous Silica Polymorphs. Microporous silicates are of great significance in the chemical industry, being used as heterogeneous catalysts in reactions such as methanol to gasoline conversion, butene and xylene isomerization, and cracking of hydrocarbons. All of these processes occur at elevated temperatures, and so understanding any changes in structure as a function of heating is relevant.

Parker and co-workers have investigated the thermal expansion of a number of zeolites and aluminophosphates using numerical free energy minimization in the zero static internal stress approximation.[37] Indeed one of the successes of lattice dynamics in this area was the prediction of negative thermal expansion for certain framework materials, which was subsequently verified experimentally.[38] This observation has been explained by Dove and co-workers using the rigid unit mode theory in which the existence of low-energy distortions can be predicted depending on the connectivity of the tetrahedra.[39,40]

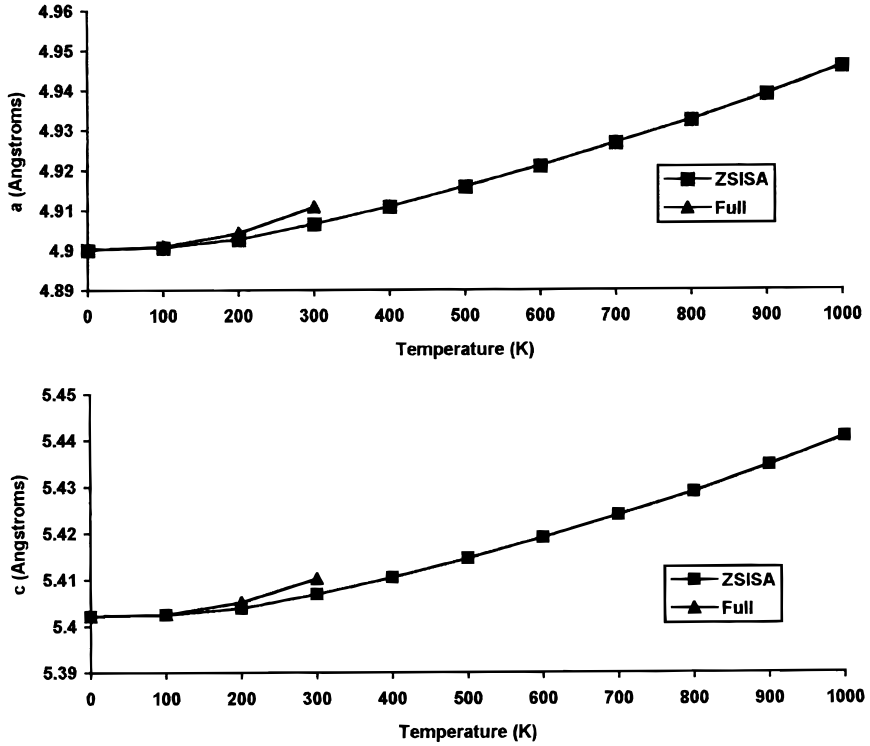

Figure 1. Plot of the calculated cell parameters (a) *a* and (b) *c* for α-quartz vs temperature based on both full and ZSISA free energy minimization.

TABLE 4: Comparison of Free Energy Minimized Structural Parameters with Those Obtained from Diffraction Studies at 13 and 296 K[30]

quartz at 13 K	experiment	full FEM	ZSISA
a (Å)	4.9021	4.9002	4.9001
c (Å)	5.3987	5.4022	5.4021
Si *x* (frac)	0.4680	0.4671	0.4672
O *x* (frac)	0.4124	0.4139	0.4136
O *y* (frac)	0.2712	0.2693	0.2696
O *z* (frac)	0.2170	0.2146	0.2150
quartz at 296 K	**experiment**	**full FEM**	**ZSISA**
a (Å)	4.9141	4.9104	4.9065
c (Å)	5.4060	5.4100	5.4069
Si *x* (frac)	0.4700	0.4701	0.4680
O *x* (frac)	0.4131	0.4151	0.4139
O *y* (frac)	0.2677	0.2644	0.2684
O *z* (frac)	0.2144	0.2105	0.2141
change in parameters	**experiment**	**full FEM**	**ZSISA**
Δ*a* (Å)	+0.0120	+0.0102	+0.0064
Δ*c* (Å)	+0.0073	+0.0079	+0.0048
Si Δ*x* (frac)	+0.0020	+0.0030	+0.0008
O Δ*x* (frac)	+0.0007	+0.0013	+0.0003
O Δ*y* (frac)	−0.0035	−0.0049	−0.0012
O Δ*z* (frac)	−0.0026	−0.0041	−0.0009

These distortions, which rely on the flexibility of the Si−O−Si angle, can lead to contraction of the solid, which offsets the smaller natural expansion of the Si−O bonds.

In this study we will consider the thermal expansion of three different microporous silicates. First, we present results for zeolite-L which was also studied by Tschaufeser and Parker[37] for comparison and to further validate the potential model. After this we will consider the application of the method to two more recently characterized materials, MCM-22 and SSZ-42.

Comparing the hexagonal unit cell parameters for zeolite-L as a function of temperature (Table 5), both sets of results show anisotropic negative thermal expansion, as found experimentally for this system, with very similar absolute cell lengths. There

TABLE 5: Comparison of the Free Energy Minimized Unit Cell Parameters for Zeolite-L Obtained by Tschaufeser and Parker[37] and This Work

temperature	ref 37		this work	
(K)	*a* (Å)	*c* (Å)	*a* (Å)	*c* (Å)
50	18.051	7.547	18.072	7.555
100	18.048	7.545	18.068	7.553
200	18.041	7.540	18.057	7.550
300	18.034	7.534	18.044	7.546
400	18.026	7.529	18.031	7.543
500	18.020	7.524	18.016	7.540

are small differences in that the new potential set yields greater thermal contraction along the *a* axis, but slightly less along the *c* axis, than the earlier shell model parameters. The absolute magnitudes of the coefficients cannot be readily compared against the experimental values, as they have only been measured for a zeolite-L sample with a significant quantity of aluminum present, plus extraframework cations. However, we can conclude that the present model accords well with the results of previous studies.

MCM-22, shown in Figure 2, is a novel microporous material, as it possesses two independent pore systems, both with 10-ring apertures, but with quite different channel shapes. Its structure was determined using a combination of high-resolution electron microscopy and synchrotron X-ray powder diffraction.[41] Although the structure could only be properly refined in the space group *P*6/*mmm*, the authors felt that this represented a thermally averaged structure due to the presence of linear Si−O−Si angles. Reducing the symmetry from hexagonal to the space group *Cmmm* was proposed, as this removed the requirement of the 180° bond angles. A recently published determination of the structure of ITQ-1, the silica analogue of MCM-22, supports the original refinement in proposing the space group *P*6/*mmm*.[42] However, it was noted that some residual electron density was present around the oxygens, which are forced by symmetry to remain on a 3-fold axis, and restraints were also needed during the refinement.

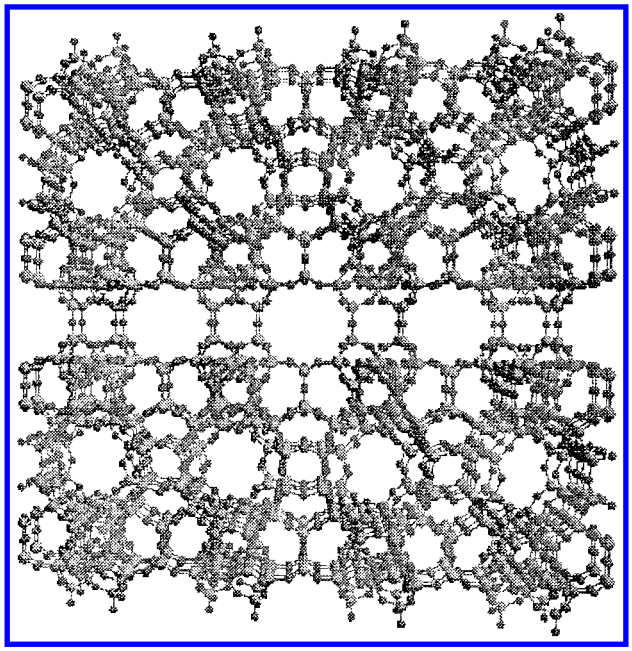

Figure 2. Structure of MCM-22.

Recently Njo et al. have used energy minimization, based on the DMM force field, to examine the question of the correct space group symmetry for MCM-22.[43] They concluded that the lowest energy structure was to be found in neither of the experimentally proposed space groups, but instead in *P*6/*m*, which maintains the linearity of the Si−O−Si angle. The authors suggested that there was the possibility that this was an artifact of the force field used, but that based on energetic trends this seemed unlikely.

We have investigated the space group symmetry and the influence of lattice dynamics on the structure of MCM-22 based on the shell model potential. In accord with the results of Njo et al. we find that an athermal minimization of both the *P*6/*mmm* and *Cmmm* structures leads to an unstable configuration. One difference is that we have actually minimized the experimental structure within the constraint of the space group, whereas Njo et al. calculated the energies at the experimental coordinates. For our potentials both minimized structures are identical within numerical precision; that is, the primitive unit cell of the orthorhombic structure returns to being hexagonal. This is the behavior that would be expected if the minimum energy structure does indeed have linear Si−O−Si bond angles. The optimized structure within either *P*6/*mmm* or *Cmmm* is characterized as having four imaginary modes at the gamma point and thus clearly wants to distort to a lower symmetry.

Analysis of the gamma point frequencies for MCM-22 in the symmetry *P*6/*m* indicates that the lowest mode that would lead to breaking of the Si−O−Si linearity is a doubly degenerate one at 36 cm^{-1}. While this is quite low, it is not the lowest frequency mode after the three translational ones. Although the equilibrium angle is 180° for the pure silica material, the presence of any defects of either an intrinsic or extrinsic nature would lead to a significant displacement of oxygen away from being linear due to the softness of this mode of distortion.

If the structure is perturbed according to the imaginary modes and then minimized using the rational function optimizer to ensure that the Hessian is positive definite, then the resulting configuration is found to have *P*6/*m* symmetry, as previously found by Njo et al. Based on athermal calculations, the *P*6/*m* structure is lower in energy than the higher symmetry form by only 0.04 kJ mol^{-1}. This difference is several orders of magnitude lower than the values reported by Njo et al. due to the optimization of the proposed experimental structures.

Turning now to consider the influence of free energy minimization on the structure of MCM-22, we find that this material demonstrates negative thermal expansion (Figure 3). While both the *a* and *c* axes contract under heating, the negative thermal expansion along the *c* direction is on the order of 4 times greater. The cell parameters calculated at 300 K are compared in Table 6 against the experimental values and those of Njo et al. Although the values predicted using the present force field and allowing for the negative thermal expansion are an improvement on the previous static calculations, the cell dimensions are still overestimated. Some of the discrepancy can be ascribed to the fact that the experimental sample contained framework boron and aluminum, as well as sodium and proton counterions.

As the temperature is increased, it might be expected that the structure of MCM-22 approaches *P*6/*mmm* symmetry in the lattice dynamical calculations, as the energy difference is small. However, if the deviation of the fractional coordinates from their idealized *P*6/*mmm* values is monitored as a function of temperature, the reverse actually occurs. Based on this, the fact that many materials appear to have higher symmetry at elevated temperatures is probably due to dynamical averaging of minima, which is not accounted for in free energy minimization.

As a final example of the application of free energy minimization to microporous silicates, we consider the recently characterized material SSZ-42, illustrated in Figure 4, which is the first example of a high-silica large-pore zeolite with an undulating one-dimensional 12-ring channel.[44] This material has a monoclinic unit cell with *C*2/*m* symmetry. Monoclinic systems have tended to be avoided for free energy minimization to date because of the greater numerical challenge of having to differentiate with respect to three cell parameters and the unique angle. Athermal optimization in this space group gives a minimum with no imaginary modes in the Brillouin zone.

Free energy minimization was performed on the primitive unit cell of SSZ-42, using a grid size of $3 \times 3 \times 6$ in reciprocal space, and then the final structural parameters were back transformed to the centered unit cell. As in the case of MCM-22, all cell lengths were found to show negative thermal expansion while the monoclinic angle increases with temperature from 102.179° at 10 K to 102.484° at 500 K.

The room-temperature structure of SSZ-42, as predicted, is compared against experiment in Table 6. The mean error in the cell parameters is about 1%, which is larger than we might expect for the potential model, and because of the absolute magnitude of the parameters, this leads to a significant difference. As SSZ-42 is highly siliceous, the discrepancy in this case is not likely to be due to framework impurities. In fact the calculated cell parameters are a closer match to the as-synthesized unit cell, when the template is still present, than to the calcined one.

A feature of the thermal behavior of SSZ-42 that we have not seen in the zero static internal stress approximation for any of the other microporous silicates run so far is that a dynamical instability appears in the Brillouin zone at a relatively low temperature. At approximately 570 K, one imaginary mode appears at (1/6, 5/6, 5/12). Because of the size of the supercell that would be required to remove this mode, it is not feasible to study the thermal expansion further. Furthermore, at temperatures just below this the anharmonic corrections are likely to be significant, at least for this one mode.

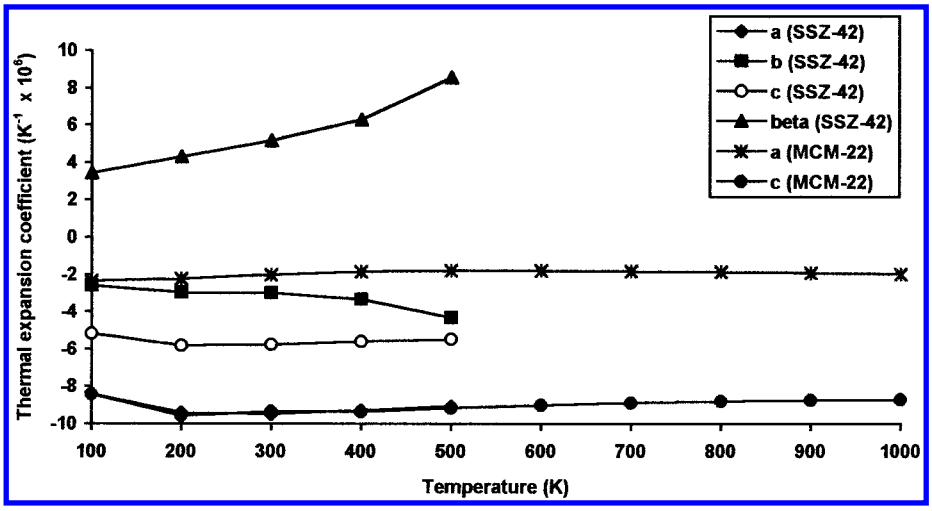

Figure 3. Plot of the thermal expansion coefficents as a function of temperature for the *a* and *c* unit cell parameters of MCM-22 and for the *a*, *b*, and *c* parameters of SSZ-42.

TABLE 6: Comparison of the Experimental Unit Cell Parameters of MCM-22 and SSZ-42 with Those Values Calculated by the Current Model Using ZSISA Free Energy Minimization at 300 K. The Statically Calculated Values for MCM-22 from Njo et al. Are Also Included for Comparison

property	experimental	this work	Njo *et al.*
MCM-22: *a* (Å)	14.1145	14.2537	14.3101
MCM-22: *c* (Å)	24.8822	24.9525	24.9940
SSZ-42: *a* (Å)	18.4991	18.6661	
SSZ-42: *b* (Å)	13.4078	13.4665	
SSZ-42: *c* (Å)	7.5755	7.6724	
SSZ-42: β (deg)	101.471	102.309	

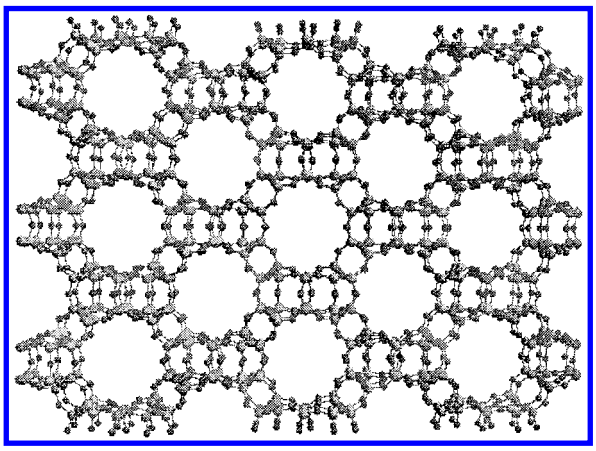

Figure 4. Structure of the high-silica microporous material SSZ-42.

4. Conclusions

Free energy minimization is an important complementary tool to molecular dynamics which allows the lower temperature regime to be explored with inclusion of vibrational quantization. A barrier to the general applicability of this technique until recently has been the computational expense and difficulties of using numerical derivatives. With the advent of efficient schemes for the analytical evaluation of forces from perturbation theory this limitation has been overcome. Analytical evaluation of all internal and strain derivatives can now be achieved at less than twice the cost of a phonon evaluation, making the analytical scheme far more efficient than existing numerical ones and potentially allowing the study of more complex materials in the future.

While in principle the analytical evaluation of derivatives allows internal degrees of freedom to also be minimized with respect to the free energy, it is found that this approach breaks down at close to room temperature for all the silicates tried so far. It is likely that this approach will only be useful for relatively rigid close packed solids where there is no possibility of internal distortions leading to imaginary modes. Hence for the majority of materials the zero static internal stress approximation must still be used unless one goes beyond the quasiharmonic approximation. Unfortunately this indicates that complete free energy minimization within the quasiharmonic approximation is unlikely to be useful for many chemical problems, such as the low-temperature study of adsorption configurations, due to the presence of low-frequency modes. For instance, a preliminary attempt to study the temperature-dependent adsorption of methane in faujasite fails at below 10 K due to the low frequency associated with the rotation of the hydrocarbon. This problem can be avoided by excluding this mode from the calculation, though this is clearly not a true solution.

For silica polymorphs we find that it is possible to derive a set of shell model potentials without a genuine three-body interaction that are at least as successful as the existing set of parameters of Sanders et al. in their ability to reproduce zeolite structures and properties. As a consequence, it is possible to maximize the efficiency of the analytical free energy derivative scheme by eliminating the need for the more expensive three-body contribution. Combined with the choice of algorithms that minimizes memory usage, this provides a practical approach to the calculation of the temperature-dependent structure of larger and more complex microporous silicates.

Acknowledgment. I thank Lev Kantorovich, Neil Allan, Mark Taylor, and co-workers for many useful discussions and preprints of their publications, as well as The Royal Society for the provision of a University Research Fellowship and funding.

References and Notes

(1) Nada, R.; Catlow, C. R. A.; Dovesi, R.; Pisani, C. *Phys. Chem. Miner.* **1990**, *17*, 353.
(2) Beck, J. S.; Vartuli, J. C.; Roth, W. J.; Leonowicz, M. E.; Kresge, C. T.; Schmitt, K. D.; Chu, C. T.-W. *J. Am. Chem. Soc.* **1992**, *114*, 10834.
(3) Thomas, J. M. *Philos. Trans. R. Soc. London A* **1990**, *333*, 173.
(4) Sanders, M. J.; Leslie, M.; Catlow, C. R. A. *J. Chem. Soc., Chem. Commun.* **1984**, 1271.
(5) Allen, M. P.; Tildesley, D. J. *Computer Simulation of Liquids*; Clarendon: Oxford, 1987.
(6) Metropolis, N.; Ulam, S. *J. Am. Statist. Ass.* **1949**, *44*, 335.

(7) Dove, M. T. *Introduction to Lattice Dynamics*; Cambridge University Press: Cambridge, 1993.
(8) Lacks, D. J.; Rutledge, G. C. *J. Chem. Phys.* **1994**, *101*, 9961.
(9) Sutton, A. P. *Philos. Trans. R. Soc. London A* **1992**, *341*, 233.
(10) Montroll, E. W. *J. Chem. Phys.* **1942**, *10*, 218.
(11) LeSar, R.; Najafabati, R.; Srolovitz, D. J. *J. Chem. Phys.* **1991**, *94*, 5090.
(12) Parker, S. C.; Price, G. D. *Adv. Solid State Chem.* **1989**, *1*, 295.
(13) Jackson, R. A.; Parker, S. C.; Tschaufeser, P. In *Modelling of Structure and Reactivity of Zeolites*; Catlow, C. R. A., Ed.; Academic Press: London, 1992.
(14) Kantorovich, L. N. *Phys. Rev. B* **1995**, *51*, 3520.
(15) Kantorovich, L. N. *Phys. Rev. B* **1995**, *51*, 3535.
(16) Taylor, M. B.; Barrera, G. D.; Allan, N. L.; Barron, T. H. K. *Phys. Rev. B* **1997**, *56*, 14380.
(17) Taylor, M. B.; Barrera, G. D.; Allan, N. L.; Barron, T. H. K.; Mackrodt, W. C. Submitted.
(18) Jackson, R. A.; Catlow, C. R. A. *Mol. Simul.* **1988**, *1*, 207.
(19) Allan, N. L.; Barron, T. H. K.; Bruno, J. A. O. *J. Chem. Phys.* **1996**, *105*, 8300.
(20) Gale, J. D. *J. Chem. Soc., Faraday Trans.* **1997**, *93*, 629.
(21) Monkhorst, H. J.; Pack, J. D. *Phys. Rev. B* **1976**, *13*, 5188.
(22) Ramirez, R.; Böhm, M. C. *Int. J. Quantum Chem.* **1988**, *34*, 571.
(23) van Beest, B. W. H.; Kramer, G. J.; van Samten, R. A. *Phys. Rev. Lett.* **1990**, *64*, 1955.
(24) Tsuneyuki, S.; Tsukada, M.; Aoki, H.; Matsui, Y. *Phys. Rev. Lett.* **1988**, *61*, 869.
(25) Dick, B. G.; Overhauser, A. W. *Phys. Rev.* **1958**, *112*, 90.
(26) Schröder, K.-P.; Sauer, J. *J. Phys. Chem.* **1996**, *100*, 11043.
(27) Eichler, U.; Kölmel, C. M.; Sauer, J. *J. Comput. Chem.* **1996**, *18*, 463.
(28) Bell, R. G.; Jackson, R. A.; Catlow, C. R. A. *J. Chem. Soc., Chem. Commun.* **1990**, 782.
(29) Gale, J. D. *Philos. Mag. B* **1996**, *73*, 3.
(30) Lager, G. A.; Jorgensen, J. D.; Rotella, F. J. *J. Appl. Phys.* **1982**, *53*, 6751.
(31) Koga, I.; Aruga, M.; Yoshinaka, Y. *Phys. Rev.* **1958**, *109*, 1467.
(32) Etchpare, J.; Merian, M.; Smetankine, L. *J. Chem. Phys.* **1974**, *60*, 1873.
(33) Kihara, K. *Eur. J. Mineral.* **1990**, *2*, 63.
(34) de Boer, K.; Jansen, A. P. J.; van Santen, R. A.; Watson, G. W.; Parker, S. C. *Phys. Rev. B* **1996**, *54*, 826.
(35) Wright, A. F.; Lehmann, M. S. *J. Solid State Chem.* **1981**, *36*, 371.
(36) Barrera, G. D.; Taylor, M. B.; Allan, N. L.; Barron, T. H. K.; Kantorovich, L. N.; Mackrodt, W. C. *J. Chem. Phys.* **1997**, *107*, 4337.
(37) Tschaufeser, P.; Parker, S. C. *J. Phys. Chem.* **1995**, *99*, 10609.
(38) Couves, J. W.; Jones, R. H.; Parker, S. C.; Tschaufeser, P.; Catlow, C. R. A. *J. Phys. Condens. Mater.* **1993**, *5*, 329.
(39) Giddy, A.; Dove, M. T.; Pawley, G. S.; Heine, V. *Acta Crystallogr.* **1993**, *A49*, 697.
(40) Hammonds, K. D.; Heine, V.; Dove, M. T. *Phase Trans. B* **1997**, *61*, 155.
(41) Leonowicz, M. E.; Lawton, J. A.; Lawton, S. L.; Rubin, M. K. *Science* **1994**, *264*, 1910.
(42) Camblor, M. A.; Corma, A.; Díaz-Cabañas, M. J.; Baerlocher, C. *J. Phys. Chem. B* **1998**, *102*, 44.
(43) Njo, S. L.; van Koningsveld, H.; van de Graaf, B. *J. Chem. Soc., Chem. Commun.* **1997**, 1243.
(44) Chen, C. Y.; Finger, L. W.; Medrud, R. C.; Crozier, P. A.; Chan, I. Y.; Harris, T. V.; Zones, S. I. *J. Chem. Soc., Chem. Commun.* **1997**, 1775.